Borasi et al. Journal of Therapeutic Ultrasound (2016) 4:32
DOI 10.1186/s40349-016-0078-3

Journal of Therapeutic Ultrasound

STUDY PROTOCOL Open Access

# Fast and high temperature hyperthermia coupled with radiotherapy as a possible new treatment for glioblastoma

Giovanni Borasi[1*], Alan Nahum[2], Margarethus M. Paulides[7], Gibin Powathil[3], Giorgio Russo[4], Laura Fariselli[5], Debora Lamia[4], Roberta Cirincione[4], Giusi Irma Forte[4], Cristian Borrazzo[8], Barbara Caccia[6], Elisabetta di Castro[8], Silvia Pozzi[6] and Maria Carla Gilardi[9]

## Abstract

**Background:** A new transcranial focused ultrasound device has been developed that can induce hyperthermia in a large tissue volume. The purpose of this work is to investigate theoretically how glioblastoma multiforme (GBM) can be effectively treated by combining the fast hyperthermia generated by this focused ultrasound device with external beam radiotherapy.

**Methods/Design:** To investigate the effect of tumor growth, we have developed a mathematical description of GBM proliferation and diffusion in the context of reaction–diffusion theory. In addition, we have formulated equations describing the impact of radiotherapy and heat on GBM in the reaction–diffusion equation, including tumor regrowth by stem cells. This formulation has been used to predict the effectiveness of the combination treatment for a realistic focused ultrasound heating scenario.
Our results show that patient survival could be significantly improved by this combined treatment modality.

**Discussion:** High priority should be given to experiments to validate the therapeutic benefit predicted by our model.

**Keywords:** Magnetic resonance-guided focused ultrasound, Hyperthermia, Oncology, Glioblastoma

## Background

Glioblastoma (GBM) is a highly aggressive tumor of the central nervous system, corresponding to grade IV of the World Health Organization's histological classification [1]. High-grade gliomas are the most common primary brain tumors in adults, with an incidence of 3.1 per 100,000 person-years in USA and with a median survival time of 14.6 months after diagnosis [2] and 11.9 months after first resection [3]. Because of their invasive nature, GBMs recur in more than 90% of patients, generally centrally [4] even if marginal and distant failures are reported [5]. The current standard treatment includes external beam radiotherapy (EBRT), maximal surgery, and chemotherapy with temozolomide (TMZ).

The standard treatments for GBM that include EBRT result in a significant increase in patient survival [6]. Dose escalation studies have demonstrated survival improvements up to an overall dose of 60 Gy [7, 8], generally with a dose fractionation of 2 Gy/day, 5 days a week, for a total of 6 weeks for the whole treatment. Beyond this dose, there is only a minimal increase in survival for severely increased toxicity [5, 9].

The study by Elaimy et al. [10] supports the use of stereotactic radiosurgery (SRS). SRS is used either to boost EBRT treatment or to treat small-volume recurrences. The addition of bevacizumab (BEV) after SRS was shown to lower the rate of tumor progression and radio-toxicity [11, 12]. The potential advantages of combining high-intensity focused ultrasound (HIFU) and radiotherapy (RT) in oncology were recently reviewed [13].

In a recent paper, Coluccia et al. [14] described the first successful non-invasive thermal ablation of a brain tumor with transcranial magnetic resonance-guided focused ultrasound (TcMRgFUS) [15]. This paper

* Correspondence: giovanni.borasi@gmail.com
[1]Department of Medicine, University of Milano Bicocca, Milano, Italy
Full list of author information is available at the end of the article

reported a tumor recurrence in the left thalamic and subthalamic region after surgery for a posteromedial temporal lobe GBM. A total of 25 sonications was applied (17 over the heat ablative threshold); the total sonication time was more than 3 h and about one tenth (0.7 $cm^3$) of the total enhancing tumor volume (6.5 $cm^3$) was ablated with an Insightec MRgFUS Exablate Neuro system [15].

The main aim of this paper is to demonstrate theoretically, as a "proof of principle", how the use of TcMRgFUS to generate "fast" hyperthermia (HT), combined with 6 weeks' EBRT therapy (one or two sessions per week, 1 h each), could have resulted in a successful treatment of the whole tumor. Our approach requires minimal or no modification of the commercially available brain sonication system [15].

## Methods/Design

### Radiotherapy and radiobiology stem cells and the new hypothesis

Several studies have been carried out in order to evaluate the radiation response of human glioma cells. The most recent and complete study on the radiobiological parameters comes from Ferrandon et al. [16]. They analyzed the photon (and carbon ion) response of eleven human-derived glioblastoma cell lines, from the most radio-resistant (T-98G with $\alpha = 0.022\ Gy^{-1}$, $\beta = 0.025\ Gy^{-2}$, $\alpha/\beta = 0.9$ Gy) to the most sensitive (U-251 with $\alpha = 0.630\ Gy^{-1}$, $\beta = 0.019\ Gy^{-2}$, $\alpha/\beta = 35$ Gy). Of course, different tumors can have a different cellular composition. Two quite recent papers [17, 18], using different data sets and methodologies, still showed similar data ([17]: $\alpha = 0.06\ Gy^{-1} \pm 0.05\ Gy^{-1}$, $\alpha/\beta = 10 \pm 15.1$ Gy, while Jones et al. [19] derive the following median values: $\alpha = 0.077\ Gy^{-1}$, $\beta = 0.009\ Gy^{-2}$, $\alpha/\beta = 9.32$ Gy). Elaborating data from Walker et al. [7], a lower sensitivity ($\alpha = 0.027\ Gy^{-1}$, $\beta = 0.0027\ Gy^{-2}$, $\alpha/\beta = 10$ Gy) was obtained [20]. Extracted from nine clinical studies, Pedicini et al. [21] obtained quite higher best estimates ($\alpha = 0.12\ Gy^{-1}$, $\beta = 0.015\ Gy^{-2}$, $\alpha/\beta = 8$ Gy). Note that these latter data include the effect of old and new drugs, such as carmustine (bischloroethylnitrosourea (BCNU)) and TMZ.

All these radiobiological data demonstrate the high resistance of glioblastoma to radiation. Still, the data are not sufficient to explain the unsatisfactory clinical results mentioned. In fact, like other tumors, glioblastoma exhibit the capability of an "adaptive response": the effect of radiation on tumor cells is not only low but becomes increasingly lower as the treatment progresses [22]. There is increasing evidence that solid tumors are hierarchically organized and contain a small population of cancer stem cells (CSCs) [23, 24]. The subpopulation of CSCs has the capability of self-renewal, an unlimited capability of proliferation and a tendency to recur [25], differing from non-stem cells (CDCs). In vitro and in animal experiments showed that the glioma CSCs were significantly more resistant than normal, differentiated cells [26].

### Mathematical modeling of GBM grow and EBRT effect

Around the late 90s [27–30], researchers recognized that the proliferative–infiltrative nature of GBM could be described mathematically by the reaction–diffusion equation [31, 32]. The possibilities offered by MR imaging confirmed the value of this description and demonstrated the significance of the two major parameters in the basic equation, namely proliferation and diffusion [33–35]. The effect of chemotherapy was introduced into the basic equation in 2003 [36] and EBRT in 2007 [20]. Several authors have considered the effects of radiation [37–43]; these approaches all considered only one tissue (i.e., cancer) diffusing into a medium (i.e., healthy brain), without any modification of the environment. Starting with Gatenby and Gawlinsky [44], the tissues (and basic equations) became twofold, representing the tumor and the environment. Their model predicted a previously unrecognized hypocellular interstitial gap at the tumor–host interface that was demonstrated both in vivo and in vitro. To solve this gap, more detailed models, with five or more equations describing the main tumor elements (such as normal, necrotic and hypoxic tumor cells, vascularity, nutrients, etc.) were subsequently proposed [45–51].

### The (Fisher–Kolmogorov) reaction–diffusion equation and tumor growth

A realistic description of GBM evolution involves two phases: first, the cells proliferate to form a small and dense lesion, then they become more diffuse and the reaction–diffusion equation can be applied [27].

The reaction–diffusion equation, including the effect of EBRT, can be written as:

$$\frac{\partial(x,t)}{\partial t} = \nabla\cdot[D(\boldsymbol{x})\nabla c(\boldsymbol{x},t)] + \rho\cdot c(x,t)\cdot\left(1-\frac{c(x,t)}{c_{\max}}\right)\Big) + R\cdot c(x,t) \tag{1}$$

where $c$ ($\boldsymbol{x}$, $t$) denotes the cell density at position $\boldsymbol{x}$ and time $t$. If B is the domain in which Eq. (1) is solved, the zero flux at the anatomic boundaries implies:

$$\boldsymbol{n}\cdot\nabla\cdot[D(\boldsymbol{x})\nabla c(\boldsymbol{x},t)] = 0\ f\ \ or\ \ \boldsymbol{x}\ \ on\ \ \partial B \tag{2}$$

where $n$ is the unit vector perpendicular to the elementary surface. To solve Eq. (1), an initial condition must be assumed, i.e., $c(0, \boldsymbol{x}) = c_o$ ($\boldsymbol{x}$). $D(\boldsymbol{x})$ is the diffusion coefficient $[l^2t^{-1}]$ and $c_{max}$ is the maximum bearable cell concentration in the tumor. A value of $c_{max} = 4.2 \times 10^8$ cells/$cm^3$ can be assumed [52], but an order of

magnitude of variation in $c_{max}$ has been reported [34, 35]. If $D(\boldsymbol{x})$ is known in a 3D volume (by using MR and/or positron emission tomography), Eqs. (1) and (2) can be solved numerically at each point of the domain. The cell-killing effect of EBRT is included through the term $R$ [$t^{-1}$], which represents the relative change of cell concentration per unit time, at time $t$. For simplicity, we apply the linear-quadratic (LQ) model [53–56]; a derivation of the $R$-term, compatible with this model, is reported in a recent paper [57].

Considering $D$ and $R$ in Eq. (4) constants, the equation depends on one single scalar radial coordinate ($r$). In the Results section, the curves 1 and 4–6 are obtained by solving this equation in one radial dimension. The tumor proliferation parameter $\rho$ is assumed to be $1.2 \times 10^{-2}$, which corresponds to a volume doubling time of 2 months (exponential growth). For the diffusion parameter $D$, a value of $5.83 \times 10^{-3}$ cm$^2$/day was previously proposed [20], which is between the values for white matter ($D_w = 1.3 \times 10^{-3}$) and gray matter ($D_G = 5 \times D_w$) [30]. This equation is solved using the PDEPE function in MATLAB (version R2010a; MathWorks, Natick, MA, USA), which applies an adaptive time-step routine. The relative and absolute tolerances for a stable solution of the equation solver are $10^{-6}$ and $10^{-9}$, respectively.

#### HIFU and hyperthermia to treat GBM

The present paper builds on the experience gained in the 70s and 90s with the development of the technology of, and the understanding of, the biological aspects obtained with "scanned ultrasound hyperthermia" [58–80] and in particular on "fast/high temperature ultrasound hyperthermia" [67, 73, 76, 79]. This latter technology may have important advantages over standard clinical hyperthermia (1 h at 42.5 °C), such as reduced dependence on perfusion and tumor inhomogeneity and a superior treatment of the tissue near large blood vessels. However, at the time, it failed to find a relevant clinical application. Our tentative explanation is that, in that period, tumor-selective visualization was not available, and the difference in the response of normal versus cancerous tissue was over-emphasized. At higher temperatures, hyperthermia-enhanced perfusion is blocked so that the best discriminating temperature was found to be 42–43 °C [81–83]. However, in the context of heat–radiation synergy, the tumor hyperthermia-enhanced perfusion is a minor effect with respect to other higher temperature cell-killing mechanisms, such as simultaneous or sequential blocking of DNA repair and aerobic and hypoxic direct cell killing [84–88]. The results of four trials [70, 74, 78, 89] of clinical HT are given in Additional file 1.

Two complete reviews on technology for hyperthermia are found in [90] and [91].

TcMRgFUS application is a promising non-invasive modality for neurosurgical intervention, but transmission of ultrasound through the skull constitutes a considerable obstacle, as already shown in the early experiments in 1950s [56]. The previously discussed experience of scanned HT demonstrated the usefulness of a new skull-specific-transduced geometry, helmet-like, with an $f$ value (radius/diameter) of about 0.5. Substantial research [92–97], including the advent of MR thermography [98–100] and phased-array transducers [101–103], led to the first pilot clinical trial of GBM ablation [15, 104]. While the temperature distribution in the brain was clearly detectable with MRI, it was impossible to reach ablation because of the limited power provided by the device. Improvements in power output have enabled ablative temperatures to be achieved, but only in a small part of the tumor [14].

In Figure five of Coluccia et al. [14], two sonication pulses with maximum temperatures of 55 °C and 58 °C, respectively, are reported as examples. For both pulses, the length of the "beam on" interval is about 13 s. The first one ($T_{max} = 55$ °C) remained under the ablation threshold ($T_{max} > 55$ °C), while the second one ($T_{max} = 58$ °C) is considered to be an ablative pulse. Both pulses are fitted with Parker's equation for the pencil beam [105, 106], using a nonlinear least squares method (Leveberg–Marquardt) as explained in the section Additional file 2.

In Fig. 1, we show the two pulse shapes mentioned by Coluccia et al. [14] and a proposed HT pulse shape. In Table 1, fitted values are reported for the following parameters: the instant of maximum temperature ($t_{max}$), the maximum temperature ($T_{max}$), and the calculated equivalent thermal dose, expressed as cumulative equivalent minutes at 43 °C ($CEM_{43}$). $C$ and $D$ are the Parker's model fitted constants.

#### Radiation plus hyperthermia response

The three human glioma cell lines (U-87MG, U-138MG, U-373MG) have a large capacity to recover from potentially lethal radiation damage. Since hyperthermia causes radiosensitization and inhibition of recovery from radiation damage, its combination with radiotherapy creates a potent combination for treating human brain tumors [22, 107–109]. In addition, Li et al. [110] and Raaphorst et al. [111] showed that HT has a greater effect on the inhibition of recovery when applied after irradiation with X-rays (RX) compared to before irradiation. In Fig. 2, we report data from Raaphorst et al. [108], in which the surviving fractions (SF) of the U-87MG cells are compared (8-h plating). Two sets of treatment were applied to the cells, radiation only (treatment A) and radiation followed by either 15 min of HT (treatment B1, $CEM_{43} = 60$ min) or 60 min. HT (Treatment B2, $CEM_{43} = 240$ min).

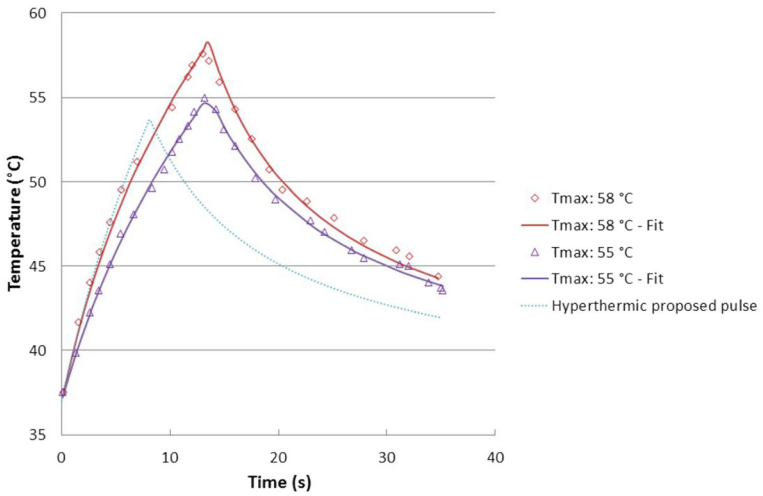


**Fig. 1** Different HIFU pulses. *Red square*: ablation pulse ($T_{max} = 58$ °C, $CEM_{43} > 240$ min); *purple triangles*: non-ablation pulse ($T_{max} = 55$ °C, $CEM_{43} < 240$ min); *dotted curve*: proposed HT pulse ($T_{max} = 53.7$ °C, $CEM_{43} = 60$ min)

In both cases, the HT was administered 5 min after the end of the irradiation. For comparison, we have added the carbon ion curve from Ferrandon et al. [16].

As is well known, carbon ions are more effective than RX (the carbon ion RBE at 10% survival is 2.57), but Fig. 2 shows that HT + RT is an extraordinarily effective combination.

Focusing on the RX plus HT 15-min curve (B1 treatment, $CEM_{43} = 60$ min), we hypothesize, as a first choice, a treatment with 3 Gy per session (SF = 0.167), two sessions per week, 6 weeks of total treatment time, with a total dose of 36 Gy. Each EBRT session should be followed, as soon as possible, by an HT treatment of the whole tumor. From Fig. 5 of Raaphorst et al. [108] and from the chosen protocol, we estimated a decrease of the sensitization effect of about 10%, for a delay of 1 h between the end of EBRT and the beginning of HT. In agreement with Raaphorst et al., we conclude that due to the greater repair capacity of cancer cells, the HT effect is expected to be more effective on tumor than on normal cells. The choice of the proposed protocols is dictated by the desire to maximize the therapeutic ratio of the treatment: reduction of healthy tissue damage but maximization of tumor effect.

**Table 1** Fitted parameters corresponding to the different HIFU pulses: the instant of maximum temperature ($t_{max}$), maximum temperature ($°C_{max}$), and the calculated equivalent thermal dose $CEM_{43}$. *C* and *D* are the Parker's fitted constants (see Additional file 2)

| Label | *t*max (s) | *T*max (°C) | $CEM_{43}$ | *C* | *D* |
|---|---|---|---|---|---|
| 58 °C | 13.01 | 57.6 | 1503.0 | 3.002 | 0.168 |
| 55 °C | 13.14 | 55.0 | 199.6 | 2.287 | 0.127 |
| HT | 8.08 | 53.7 | 60.0 | 3.002 | 0.127 |

Note for the proposed protocols (B1 and B2) the following six points:

1. The total EBRT dose and fractionation should be acceptable, since α and β as previously given will lead to a lower biological effective dose than the "standard protocol" (2 Gy per session, five sessions per week, 6 weeks total treatment time. Maximum total dose is 60 Gy)
2. Exploiting the time interval of 2–3 days between the treatments, the phenomenon of thermo-resistance due to heat shock proteins (HSP) that can reduce the treatment effect, is avoided [112]
3. The induction of the immunogenic tumor cells and direct tumor cell killing by HT in combination with EBRT can contribute to immune activation against the tumor [113]
4. Thanks to the nearly constant sensitivity to RX plus HT of CSCs and CDCs found for the cell lines evaluated [114], the problem of resistant sub-populations should be avoided
5. The effect of (mild) HT on hypoxic tumor regions is well known [115, 116], and there are several indications that this effect is similar or stronger at higher temperatures [117, 118]
6. In treatment B2, only one session per week is required, given the increased dose (4.4 Gy × 6)

Clearly, the main limitation of the treatment described in Coluccia et al. [14] is the time required to alleviate the pain to the brain of the patient, requiring long cooling intervals between the sonication. This pain is mainly due to the heat energy absorbed by the bone (30–60 times more than by the soft tissue [119]). With the

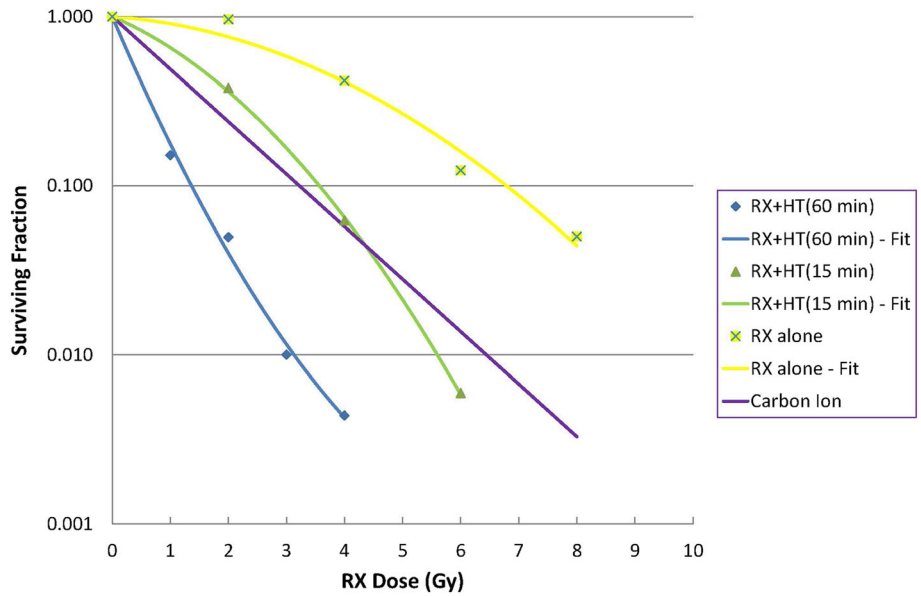


**Fig. 2** Surviving fraction of U-87MG cells for different radiation qualities. *Yellow crosses*: RX alone (treatment A); *purple line*: carbon ions (curve drawn from Ferrandon et al. [16]); *green triangles*: RX + HT 15 min (treatment B1); *blue diamonds*: RX + HT 60 min (treatment B2).

proposed HT pulses, the warming of the whole T1w-enhancing tumor would require 163 pulses, for a total time of 1.27 h (each pulse consisting of 8.1 s of beam on and 20 s of "beam off", i.e., cooling down time). The cooling down interval has been here calculated on the basis of HIFU ablative literature [14, 120, 121] and still requires experimental verification. Let us consider another example: a tumor with an equivalent radius of 2.3 cm (volume of 51 $cm^3$) of which about 92% of the volume was removed by surgery. The residual tumor, i.e., our target, is therefore 4.2 $cm^3$. This requires about 105 sonications with 8.1 s of beam on time. The total treatment time would be less than 1 h (49.2 min).

## Results

In this section, we compare the tumor cell survival corresponding to the different treatments (Table 2 and Fig. 3).

Note that the "standard" treatment (2 Gy × 30, N.1 in Table 1, dash-dotted orange line in Fig. 3) is calculated neglecting the stem cell effect (only EBRT–RX). Due to the presence of cancer stem cells, this treatment should be considered unrealistic.

Curves 2 and 3 (solid and dotted blue lines, respectively, in Fig. 3) include the effect of the CSC cells [122]. The exceptional resistance of CSCs and the interplay of these cells with CDC progressively reduces the rate of decrease of the cancer cells ("adaptive response"). The clinical data are reproduced reasonably well by the LQ model when assuming lower α and β values (curve 4, solid green line, in Fig. 3). This model is applied to both CSCs and CDCs. The fraction of CSCs in the total cell number ($F$) is assumed to be $1.6 \times 10^{-2}$. Curve 4 was previously calculated [20] using Eq. (4) and clinical radiobiological data [7]. It is interesting to note that this curve, by assuming very low values for α and β, reproduces quite well the "time to offset" (i.e., the time for the tumor volume to grow back to its initial volume) of the previous curves that are based on the effect of CSCs. Curves 5 and 6 in Table 2 (purple solid and red dotted lines in Fig. 3) show the effect of the new RX + HT treatments. Curve 5 corresponds to protocol B1, with two sessions a week (for example, Monday and Thursday), in which, after conformal RT with a maximum dose of 3 Gy, HT is administered with a $CEM_{43}$ of 60 min. Curve 6 corresponds to protocol B2: one session a week with a larger radiation dose (4.7 Gy) and the same thermal dose ($CEM_{43}$ = 60 min). Curves n. 5 and 6 are calculated with 1-h delay between the end of RT and the beginning of HT. Curves 7 and 8 are calculated respectively as curves n. 5 and 6, but with 2-h delay between the end of RT and the beginning of HT.

## Discussion and conclusions

As is clear from Table 2 and Fig. 3, the proposed protocols with RX + HT easily outperform the traditional ones; they lead to a low survival level of tumor cells and a long offset time such that the patient is effectively cured, in contrast to glioblastoma treatment today where cure is never achieved. At very low levels of cell survival, the immune system may also play an important role [123]. To our knowledge, the proposed methodology is

**Table 2** Parameter values along with bibliographic references of the curves shown in Fig. 3. "Time to offset" is the time for the tumor to come back to the initial value. Curves n. 5 and 6 are calculated with 1-h delay between the end of RT and the beginning of HT. Curves 7 and 8 are calculated with 2-h delay between the end of RT and the beginning of HT

| Number | Title | α ($Gy^{-1}$) | β ($Gy^{-2}$) | Minimum survival value | Time to offset | Reference |
|---|---|---|---|---|---|---|
| 1 | Only RX (unrealistic) | $5.4 \times 10^{-2}$ | $4.2 \times 10^{-2}$ | $3.61 \times 10^{-4}$ | 2.29 years | [108] |
| 2 | Yu 2 Gy × 30–CSCs | $1 \times 10^{-2}$ $1.25 \times 10^{-1}$ | $1.77 \times 10^{-7}$ $2.8 \times 10^{-2}$ | $1.66 \times 10^{-2}$ | 210 days | [122] |
| 3 | Yu–Extrapolated | $1 \times 10^{-2}$ $1.25 \times 10^{-1}$ | $1.77 \times 10^{-7}$ $2.8 \times 10^{-2}$ | – | – | Extrapolation of the previous SF |
| 4 | Powathil 2 Gy × 30 | $2.7 \times 10^{-2}$ | $2.7 \times 10^{-3}$ | $1.89 \times 10^{-1}$ | 226 days | [20] |
| 5 | RX + HT 3 Gy × 12–1 h | $3.36 \times 10^{-1}$ | $8.7 \times 10^{-2}$ | $2.897 \times 10^{-8}$ | 4.61 years | [108] |
| 6 | RX + HT 4.7 Gy × 6–1 h | $3.36 \times 10^{-1}$ | $8.7 \times 10^{-2}$ | $4.986 \times 10^{-8}$ | 4.48 years | [108] |
| 7 | RX + HT 3 Gy × 12–2 h | $3.36 \times 10^{-1}$ | $8.7 \times 10^{-2}$ | $3.286 \times 10^{-7}$ | 4.02 years | [108] |
| 8 | RX + HT 4.7 Gy × 6–2 h | $3.36 \times 10^{-1}$ | $8.7 \times 10^{-2}$ | $4.986 \times 10^{-7}$ | 3.91 years | [108] |

the only one capable of achieving curative outcomes. In addition, we wish to emphasize that we used the $CEM_{43}$ concept [124] to establish an equivalence, in terms of the total cell-killing effect, between the Raaphorst data [108] obtained at 45 °C and the hypothesized HT pulse shape of Fig. 1. This choice doesn't take into account radiation–heat synergy. In this regard, Law [125] found that for heat combined with X-rays, the time required to produce a given level of radiodermatitis was reduced by a factor of three for a rise in temperature of 1° (in comparison with the Sapareto and Dewey [124] law, which predicts a factor of two). Even if the law result was obtained in a different tissue, our data could be an underestimation, and a pulse shape with a lower HT maximum temperature and/or a lower time length can be possible in practice. Of course, on this point, direct experimental data are required. In any case, the illustrated results can be obtained without significant modification of the present system. Regarding the two proposed protocols, only experience will help to choose between them: B2 is easier to execute in clinical practice (just one session a week) but it is not clear if we would have the same benefits from the clinical point of view (oxygenation and immune system stimulation).

It is important to emphasize that the equivalent doses [56] of the two proposed treatments are more than 35% lower than the "reference" dose of 60 Gy, given in 2 Gy fractions, five days a week for a total time of 6 weeks. This very important consequence of the proposed scheduling would reduce drastically the radiation damage to surrounding healthy tissues, evaluated in terms of normal tissue complication probabilities [126]. To achieve a uniform treatment of the target volume, as for ablation, the HT spots can be spaced in a raster by superimposing

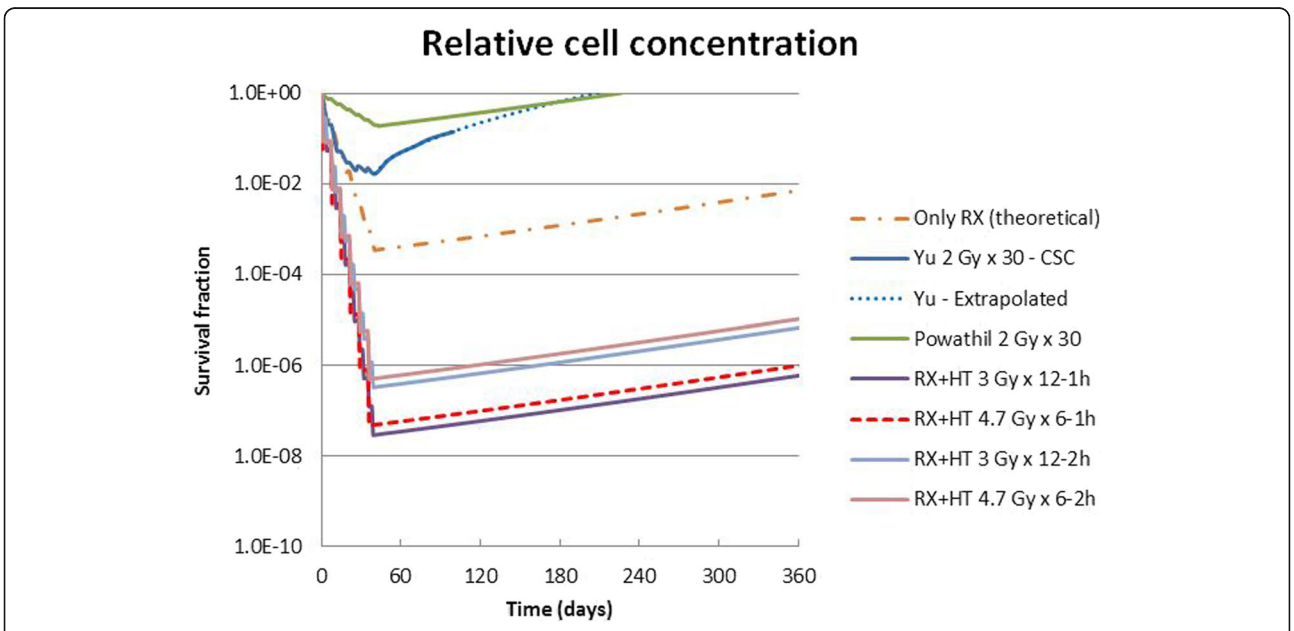


**Fig. 3** Comparison of relative glioblastoma cell survival by using different treatments, as illustrated in Table 2

the isolines (or, better, isosurfaces) 50% of the thermal dose. There is no reason for the 50% isolines of our HT to have a different shape or location compared to the ablation treatment (Additional file 3).

The main limitation of our proposed treatment is that the tumor volume assumed in our modeling only measures about 4–6 $cm^3$. However, in the light of the groundbreaking results described in this paper, maximum effort must be made to extend the size of the tumor mass that we can cure. It can be noted that we haven't considered methods for drastically lowering the frequency (220 kHz) to open the blood–brain barrier (BBB) and improve drug delivery [127–130], with the use of microbubbles [131, 132], nanoparticles [133–135], or contrast media [136]. Such a strategy is highly problematic [137, 138].

The proposed treatment can increase the treated region by using at least two different techniques.

Firstly: in the presence of radiation, the Sapareto–Dewey law [124] may no longer be valid, and a different model should be used to establish the time–temperature equivalence. If we follow the Law [125] expression (for every 1° increase, one third (not a half) of the time required for the same effect), the maximum temperature of the HT pulse in Fig. 1 would be less than 50 °C, and the useful impulse length would be about 6 s instead of about 8 s (for the same effect). In addition, a lower temperature HT pulse would require a lower ultrasonic (US) intensity, which means a lower pressure. In turn, a lower pressure on the skull would allow, at the same level of safety with respect to a possible cavitation event, a lower frequency. This latter would give a better US transmission and a lower temperature on the skull, thereby reducing the cooling time and allowing a larger target volume to be treated.

Secondly: making better use of the heat that flows, inside the target, from higher to lower temperature regions. In this regard, different methods are described in the literature of covering the tumor volume [139–143] more efficiently than the point-by-point strategy adopted here for simplicity.

In addition, it is important to consider correctly the evolution of GBM. All the three more complete GBM models mentioned in the text [47, 48, 51] predict that in the evolution of the disease, the biologically active region (proliferating and infiltrating) is pushed toward the periphery of the tumor, while the central part becomes progressively larger and necrotic. Therefore, it seems reasonable to concentrate in this peripheral region both radiation and HT. This would change radically the GBM treatment planning and would reduce significantly the region to be heated (and irradiated) [144].

In light of the above, there is significant room for improvement of the proposed technique.

As has been emphasized in relation to the results obtained, these new implementations also require careful experimental validation, but the door is open for a truly effective and, possibly, life-saving GBM treatment.

Addendum: this paper is dedicated, in particular, to our friends Mario Granata and Luciano Andreucci, who died from this devastating disease.

## Additional files

**Additional file 1:** Reports the results of four trials of clinical HT. (DOCX 18 kb)

**Additional file 2:** Reports US pulses fitted with the Parker's equation, using nonlinear least squared method. (DOCX 21 kb)

**Additional file 3:** Location of isolines in ablative and HT US pulses. (DOCX 19 kb)

#### Abbreviations

BCNU: Bis-chloroethylnitrosourea; BEV: Bevacizumab; CDCs: Non-cancer stem cells; $CEM_{43}$: Cumulative equivalent minutes at 43 °C; CSCs: Cancer stem cells; EBRT: External beam radiotherapy; FUS: Focused ultrasound; GBM: Glioblastoma; HIFU: High-intensity focused ultrasound; HT: Hyperthermia; RT: Radiotherapy; RX: X-rays; SRS: Stereotactic radiosurgery; TcMRgFUS: Transcranial magnetic resonance-guided focused ultrasound; TMZ: Temolozomide

#### Acknowledgements

We are grateful to the referees for their constructive comments which have helped us to clarify several points in the text.

#### Funding

No funding for this research has been received.

#### Availability of data and materials

Data sharing not applicable to this article as no dataset were generated or analyzed during the current study.

#### Authors' contributions

GB, AN, MP, GP, GR, and MG conceived the study. LF, RC, and GF provided the clinical and biological rationale. CB, BC, and EC helped with the calculations. DL and SP prepared the manuscript. All authors read, approved, and contributed to the final manuscript.

#### Competing interests

The authors declare that they have no competing interests.

#### Consent for publication

Not applicable.

#### Ethics approval and consent to participate

Not applicable.

#### Author details

[1]Department of Medicine, University of Milano Bicocca, Milano, Italy. [2]Physics Department, Liverpool University, Liverpool, UK. [3]Department of Mathematics, College of Science, Swansea University, Swansea, UK. [4]Istituto di Bioimmagini e Fisiologia Molecolare–Consiglio Nazionale delle Ricerche, Palermo, Italy. [5]Istituto Nazionale Neurologico "C.Besta", Milan, Italy. [6]Istituto Superiore di Sanità, Rome, Italy. [7]Erasmus MC Cancer Institute, Rotterdam, The Netherlands. [8]Sapienza University of Rome, Rome, Italy. [9]Istituto di Bioimmagini e Fisiologia Molecolare–Consiglio Nazionale delle Ricerche, Milan, Italy.

Received: 20 April 2016 Accepted: 18 November 2016
Published online: 08 December 2016

#### References

1. Louis DN, et al. The 2007 WHO classification of tumours of the central nervous system. Acta Neuropathol. 2007;114(2):97–109.

2. Stupp R, et al. Radiotherapy plus concomitant and adjuvant temozolomide for glioblastoma. N Engl J Med. 2005;352(10):987–96.
3. Quick J, et al. Benefit of tumor resection for recurrent glioblastoma. J Neurooncol. 2014;117(2):365–72.
4. Chang SM, et al. Patterns of care for adults with newly diagnosed malignant glioma. JAMA. 2005;293(5):557–64.
5. Paulsson AK, et al. Limited margins using modern radiotherapy techniques does not increase marginal failure rate of glioblastoma. Am J Clin Oncol. 2014;37(2):177–81.
6. Walker MD, et al. Randomized comparisons of radiotherapy and nitrosoureas for the treatment of malignant glioma after surgery. N Engl J Med. 1980;303(23):1323–9.
7. Walker MD, Strike TA, Sheline GE. An analysis of dose-effect relationship in the radiotherapy of malignant gliomas. Int J Radiat Oncol Biol Phys. 1979;5(10):1725–31.
8. Badiyan SN, et al. Radiation therapy dose escalation for glioblastoma multiforme in the era of temozolomide. Int J Radiat Oncol Biol Phys. 2014;90(4):877–85.
9. Morris DE, Kimple RJ. Normal tissue tolerance for high-grade gliomas: is it an issue? Semin Radiat Oncol. 2009;19(3):187–92.
10. Elaimy AL, et al. Clinical outcomes of gamma knife radiosurgery in the salvage treatment of patients with recurrent high-grade glioma. World Neurosurg. 2013;80(6):872–8.
11. Park KJ, et al. Salvage gamma knife stereotactic radiosurgery followed by bevacizumab for recurrent glioblastoma multiforme: a case–control study. J Neurooncol. 2012;107(2):323–33.
12. Ney DE, et al. Phase II trial of hypofractionated intensity-modulated radiation therapy combined with temozolomide and bevacizumab for patients with newly diagnosed glioblastoma. J Neurooncol. 2015;122(1):135–43.
13. Borasi G, et al. High-intensity focused ultrasound plus concomitant radiotherapy: a new weapon in oncology? J Ther Ultrasound. 2013;1(6):1–4.
14. Coluccia D, et al. First noninvasive thermal ablation of a brain tumor with MR-guided focused ultrasound. J Ther Ultrasound. 2014;2:17.
15. Insightec, TC, Israel. http://www.insightec.com/clinical/neurosurgery. Exablate Neuro.
16. Ferrandon S, et al. Cellular and molecular portrait of eleven human glioblastoma cell lines under photon and carbon ion irradiation. Cancer Lett. 2015;360(1):10–6.
17. Qi XS, Schultz CJ, Li XA. An estimation of radiobiologic parameters from clinical outcomes for radiation treatment planning of brain tumor. Int J Radiat Oncol Biol Phys. 2006;64(5):1570–80.
18. Jones B, Sanghera P. Estimation of radiobiologic parameters and equivalent radiation dose of cytotoxic chemotherapy in malignant glioma. Int J Radiat Oncol Biol Phys. 2007;68(2):441–8.
19. Yu T, Wang Z, Mason TJ. A review of research into the uses of low level ultrasound in cancer therapy. Ultrason Sonochem. 2004;11(2):95–103.
20. Powathil G, et al. Mathematical modeling of brain tumors: effects of radiotherapy and chemotherapy. Phys Med Biol. 2007;52(11):3291–306.
21. Pedicini P, et al. Clinical radiobiology of glioblastoma multiforme: estimation of tumor control probability from various radiotherapy fractionation schemes. Strahlenther Onkol. 2014;190(10):925–32.
22. Smith DM, Raaphorst GP. Adaptive responses in human glioma cells assessed by clonogenic survival and DNA strand break analysis. Int J Radiat Biol. 2003;79(5):333–9.
23. Reya T, et al. Stem cells, cancer, and cancer stem cells. Nature. 2001; 414(6859):105–11.
24. Pajonk F, Vlashi E, McBride WH. Radiation resistance of cancer stem cells: the 4 R's of radiobiology revisited. Stem Cells. 2010;28(4):639–48.
25. Clarke MF, et al. Cancer stem cells—perspectives on current status and future directions: AACR Workshop on cancer stem cells. Cancer Res. 2006;66(19):9339–44.
26. Bao S, et al. Glioma stem cells promote radioresistance by preferential activation of the DNA damage response. Nature. 2006;444(7120):756–60.
27. Tracqui P, et al. A mathematical model of glioma growth: the effect of chemotherapy on spatio-temporal growth. Cell Prolif. 1995;28(1):17–31.
28. Woodward DE, et al. A mathematical model of glioma growth: the effect of extent of surgical resection. Cell Prolif. 1996;29(6):269–88.
29. Burgess PK, et al. The interaction of growth rates and diffusion coefficients in a three-dimensional mathematical model of gliomas. J Neuropathol Exp Neurol. 1997;56(6):704–13.
30. Swanson KR, Alvord Jr EC, Murray JD. A quantitative model for differential motility of gliomas in grey and white matter. Cell Prolif. 2000;33(5):317–29.
31. Fisher RA. The wave of advance of advantageous genes. Ann Eugenics. 1937;7:353–69.
32. Kolmogorov A, Petrovskii I, Piscounov N. A study of the diffusion equation with increase in the amount of substance, and its application to a biological problem. Bull Moskow University Math Mech. 1937;1:1–25.
33. Harpold HL, Alvord Jr EC, Swanson KR. The evolution of mathematical modeling of glioma proliferation and invasion. J Neuropathol Exp Neurol. 2007;66(1):1–9.
34. Swanson KR, et al. Velocity of radial expansion of contrast-enhancing gliomas and the effectiveness of radiotherapy in individual patients: a proof of principle. Clin Oncol (R Coll Radiol). 2008;20(4):301–8.
35. Wang CH, et al. Prognostic significance of growth kinetics in newly diagnosed glioblastomas revealed by combining serial imaging with a novel biomathematical model. Cancer Res. 2009;69(23):9133–40.
36. Murray JD. Mathematical Biology I and II Interdisciplinary Applied Mathematics. 3rd ed. Berlin: Springer; 2003.
37. Rockne R, et al. A mathematical model for brain tumor response to radiation therapy. J Math Biol. 2009;58(4–5):561–78.
38. Rockne R, et al. Predicting the efficacy of radiotherapy in individual glioblastoma patients in vivo: a mathematical modeling approach. Phys Med Biol. 2010;55(12):3271–85.
39. Holdsworth CH, et al. Adaptive IMRT using a multiobjective evolutionary algorithm integrated with a diffusion-invasion model of glioblastoma. Phys Med Biol. 2012;57(24):8271–83.
40. Roniotis A, et al. Simulating radiotherapy effect in high-grade glioma by using diffusive modeling and brain atlases. J Biomed Biotechnol. 2012;2012:715812.
41. Corwin D, et al. Toward patient-specific, biologically optimized radiation therapy plans for the treatment of glioblastoma. PLoS One. 2013;8(11), e79115.
42. Rockne RC, et al. A patient-specific computational model of hypoxia-modulated radiation resistance in glioblastoma using 18 F-FMISO-PET. J R Soc Interface. 2015;12:20141174.
43. Borasi G, Nahum AE. Comment on "simulating radiotherapy effect in high-grade glioma by using diffusive modeling and brain atlases". Biomed Res Int. 2015;2015.
44. Gatenby RA, Gawlinski ET. A reaction–diffusion model of cancer invasion. Cancer Res. 1996;56(24):5745–53.
45. Eikenberry SE, et al. Virtual glioblastoma: growth, migration and treatment in a three-dimensional mathematical model. Cell Prolif. 2009;42(4):511–28.
46. Hawkins-Daarud A, et al. Modeling tumor-associated edema in gliomas during anti-angiogenic therapy and its impact on imageable tumor. Front Oncol. 2013;3:66.
47. Papadogiorgaki M, et al. Mathematical modelling of spatio-temporal glioma evolution. Theor Biol Med Model. 2013;10:47.
48. Swanson KR, et al. Quantifying the role of angiogenesis in malignant progression of gliomas: in silico modeling integrates imaging and histology. Cancer Res. 2011;71(24):7366–75.
49. Colombo MC, et al. Towards the personalized treatment of glioblastoma: integrating patient-specific clinical data in a continuous mechanical model. PLoS One. 2015;10(7), e0132887.
50. Colombo MC, et al. Correction: towards the personalized treatment of glioblastoma: integrating patient-specific clinical data in a continuous mechanical model. PLoS One. 2015;10(11), e0143032.
51. Scribner E, et al. Effects of anti-angiogenesis on glioblastoma growth and migration: model to clinical predictions. PLoS One. 2014;9(12), e115018.
52. Stein AM, et al. A mathematical model of glioblastoma tumor spheroid invasion in a three-dimensional in vitro experiment. Biophys J. 2007;92(1):356–65.
53. Kellerer AM, Rossi HH. RBE and the primary mechanism of radiation action. Radiat Res. 1971;47(1):15–34.
54. Kellerer AM, Rossi HH. Statistical aspects of the survival curve. Curr Topics Radiat Res. 1972;8:85–158.
55. Kellerer AM, Rossi HH. A generalized formulation of dual radiation action. Radiat Res. 2012;178(2):AV204–13.
56. Thames HD. An 'incomplete-repair' model for survival after fractionated and continuous irradiations. Int J Radiat Biol Relat Stud Phys Chem Med. 1985;47(3):319–39.
57. Borasi G, Nahum A. Modelling the radiotherapy effect in the reaction–diffusion equation. 2016. Phys Med.
58. Lele PP. Induction of Deep, Local Hyperthermia by and Electromagnetic Fields. Radiat. Environ. Biophys. 1980;17:205-17.
59. Hynynen K, Watmough DJ, Mallard JR. Design of ultrasonic transducers for local hyperthermia. Ultrasound Med Biol. 1981;7(4):397–402.
60. Hynynen K, Watmough DJ, Mallard JR. The effects of some physical factors on the production of hyperthermia by ultrasound in neoplastic tissues. Radiat Environ Biophys. 1981;19(3):215–26.

61. ter Haar G, Hopewell JW. The induction of hyperthermia by ultrasound: its value and associated problems. I. Single, static, plane transducer. Phys Med Biol. 1983;28(8):889–96.
62. ter Haar G, Hopewell JW. The induction of hyperthermia by ultrasound; its value and associated problems: II. Scanned-plane transducer. Phys Med Biol. 1985;30(12):1327–33.
63. Tobias J, et al. An ultrasound window to perform scanned, focused ultrasound hyperthermia treatments of brain tumors. Med Phys. 1987;14(2):228–34.
64. Hynynen K. Demonstration of enhanced temperature elevation due to nonlinear propagation of focussed ultrasound in dog's thigh in vivo. Ultrasound Med Biol. 1987;13(2):85–91.
65. Hynynen K, et al. A scanned, focused, multiple transducer ultrasonic system for localized hyperthermia treatments. Int J Hyperthermia. 1987;3(1):21–35.
66. Moros EG, Roemer RB, Hynynen K. Simulations of scanned focused ultrasound hyperthermia. the effects of scanning speed and pattern on the temperature fluctuations at the focal depth. IEEE Trans Ultrason Ferroelectr Freq Control. 1988;35(5):552–60.
67. Billard BE, Hynynen K, Roemer RB. Effects of physical parameters on high temperature ultrasound hyperthermia. Ultrasound Med Biol. 1990;16(4):409–20.
68. Lin WL, Roemer RB, Hynynen K. Theoretical and experimental evaluation of a temperature controller for scanned focused ultrasound hyperthermia. Med Phys. 1990;17(4):615–25.
69. Johnson C, et al. Multi-point feedback control system for scanned, focused ultrasound hyperthermia. Phys Med Biol. 1990;35(6):781–6.
70. Guthkelch AN, et al. Treatment of malignant brain tumors with focused ultrasound hyperthermia and radiation: results of a phase I trial. J Neurooncol. 1991;10(3):271–84.
71. Hynynen K. The threshold for thermally significant cavitation in dog's thigh muscle in vivo. Ultrasound Med Biol. 1991;17(2):157–69.
72. Roemer RB. Optimal power deposition in hyperthermia. I. The treatment goal: the ideal temperature distribution: the role of large blood vessels. Int J Hyperthermia. 1991;7(2):317–41.
73. Dorr LN, Hynynen K. The effects of tissue heterogeneities and large blood vessels on the thermal exposure induced by short high-power ultrasound pulses. Int J Hyperthermia. 1992;8(1):45–59.
74. Stea B, et al. Treatment of malignant gliomas with interstitial irradiation and hyperthermia. Int J Radiat Oncol Biol Phys. 1992;24(4):657–67.
75. Lin WL, et al. Optimization of temperature distributions in scanned, focused ultrasound hyperthermia. Int J Hyperthermia. 1992;8(1):61–78.
76. Damianou C, Hynynen K. Focal spacing and near-field heating during pulsed high temperature ultrasound therapy. Ultrasound Med Biol. 1993;19(9):777–87.
77. Anhalt DP, Hynynen K, Roemer RB. Patterns of changes of tumour temperatures during clinical hyperthermia: implications for treatment planning, evaluation and control. Int J Hyperthermia. 1995;11(3):425–36.
78. Sneed PK, et al. Survival benefit of hyperthermia in a prospective randomized trial of brachytherapy boost +/− hyperthermia for glioblastoma multiforme. Int J Radiat Oncol Biol Phys. 1998;40(2):287–95.
79. Britt RH, Pounds DW, Lyons BE. Feasibility of treating malignant brain tumors with focused ultrasound. Prog Exp Tumor Res. 1984;28:232–45.
80. Hunt JW, et al. Rapid heating: critical theoretical assessment of thermal gradients found in hyperthermia treatments. Int J Hyperthermia. 1991;7(5):703–18.
81. Dudar TE, Jain RK. Differential response of normal and tumor microcirculation to hyperthermia. Cancer Res. 1984;44(2):605–12.
82. Fukumura D, Jain RK. Imaging angiogenesis and the microenvironment. Apmis. 2008;116(7–8):695–715.
83. Song CW, Park H, Griffin RJ. Improvement of tumor oxygenation by mild hyperthermia. Radiat Res. 2001;155(4):515–28.
84. Sapareto SA, Hopwood LE, Dewey WC. Combined effects of X irradiation and hyperthermia on CHO cells for various temperatures and orders of application. Radiat Res. 1978;73(2):221–33.
85. Dewey WC, et al. Cellular responses to combinations of hyperthermia and radiation. Radiology. 1977;123(2):463–74.
86. Overgaard J. Simultaneous and sequential hyperthermia and radiation treatment of an experimental tumor and its surrounding normal tissue in vivo. Int J Radiat Oncol Biol Phys. 1980;6(11):1507–17.
87. Iliakis G, Wu WQ, Wang ML. DNA double strand break repair inhibition as a cause of heat radiosensitization: Re-evaluation considering backup pathways of NHEJ. Int J Hyperthermia. 2008;24(1):17–29.
88. Crezee H, et al. Thermoradiotherapy planning: integration in routine clinical practice. Int J Hyperthermia. 2016;32(1):1–9.
89. Maier-Hauff K, et al. Efficacy and safety of intratumoral thermotherapy using magnetic iron-oxide nanoparticles combined with external beam radiotherapy on patients with recurrent glioblastoma multiforme. J Neurooncol. 2011;103(2):317–24.
90. Diederich CJ, Hynynen K. Ultrasound technology for hyperthermia. Ultrasound Med Biol. 1999;25(6):871–87.
91. Lee Titsworth W, et al. Fighting fire with fire: the revival of thermotherapy for gliomas. Anticancer Res. 2014;34(2):565–74.
92. Hynynen K, Jolesz FA. Demonstration of potential noninvasive ultrasound brain therapy through an intact skull. Ultrasound Med Biol. 1998;24(2):275–83.
93. Aubry JF, et al. Experimental demonstration of noninvasive transskull adaptive focusing based on prior computed tomography scans. J Acoust Soc Am. 2003;113(1):84–93.
94. Hynynen K, et al. 500-element ultrasound phased array system for noninvasive focal surgery of the brain: a preliminary rabbit study with ex vivo human skulls. Magn Reson Med. 2004;52(1):100–7.
95. Lin WL, et al. Treatable domain and optimal frequency for brain tumors during ultrasound hyperthermia. Int J Radiat Oncol Biol Phys. 2000;46(1):239–47.
96. Cline HE, et al. MR-guided focused ultrasound surgery. J Comput Assist Tomogr. 1992;16(6):956–65.
97. Pulkkinen A, et al. Numerical simulations of clinical focused ultrasound functional neurosurgery. Phys Med Biol. 2014;59(7):1679–700.
98. Ishihara Y, et al. A precise and fast temperature mapping using water proton chemical shift. Magn Reson Med. 1995;34(6):814–23.
99. Rieke V, Butts Pauly K. MR thermometry. J Magn Reson Imaging. 2008;27(2):376–90.
100. Borman PT, et al. Towards real-time thermometry using simultaneous multislice MRI. Phys Med Biol. 2016;61(17):N461–77.
101. Cain CA and S Umemura. Annular and sector phased array applicators for ultrasound hyperthermia. in 1985 ieee ultrasonic symposium. 1985.
102. Daum RD, et al. Design and evaluation of a feedback based phased array system for ultrasound surgery. IEEE Trans Ultrason Ferroelectr Freq Control. 1998;45(2):431–7.
103. Hynynen K, Jones RM. Image-guided ultrasound phased arrays are a disruptive technology for non-invasive therapy. Phys Med Biol. 2016;61(17):R206–48.
104. McDannold N, et al. Transcranial magnetic resonance imaging- guided focused ultrasound surgery of brain tumors: initial findings in 3 patients. Neurosurgery. 2010;66(2):323–32.
105. Parker KJ. Effects of heat conduction and sample size on ultrasonic absorption measurements. J Acoust Soc Am. 1985;77(2):719–25.
106. Dillon CR, et al. An analytical solution for improved HIFU SAR estimation. Phys Med Biol. 2012;57(14):4527–44.
107. Raaphorst GP, et al. A comparison of heat and radiation sensitivity of three human glioma cell lines. Int J Radiat Oncol Biol Phys. 1989;17(3):615–22.
108. Raaphorst GP, et al. Hyperthermia enhancement of radiation response and inhibition of recovery from radiation damage in human glioma cells. Int J Hyperthermia. 1991;7(4):629–41.
109. Raaphorst GP, et al. A comparison of the enhancement of radiation sensitivity and DNA polymerase inactivation by hyperthermia in human glioma cells. Radiat Res. 1993;134(3):331–6.
110. Li GC, Evans RG, Hahn GM. Modification and inhibition of repair of potentially lethal x-ray damage by hyperthermia. Radiat Res. 1976;67(3):491–501.
111. Raaphorst GP, Azzam EI, Feeley M. Potentially lethal radiation damage repair and its inhibition by hyperthermia in normal hamster cells, mouse cells, and transformed mouse cells. Radiat Res. 1988;113(1):171–82.
112. Rylander MN, et al. Measurement and mathematical modeling of thermally induced injury and heat shock protein expression kinetics in normal and cancerous prostate cells. Int J Hyperthermia. 2010;26(8):748–64.
113. Frey B, et al. Old and new facts about hyperthermia-induced modulations of the immune system. Int J Hyperthermia. 2012;28(6):528–42.
114. Man J, et al. Hyperthermia sensitizes glioma stem-like cells to radiation by inhibiting AKT signaling. Cancer Res. 2015;75(8):1760–9.
115. Sun X, et al. The effect of mild temperature hyperthermia on tumour hypoxia and blood perfusion: relevance for radiotherapy, vascular targeting and imaging. Int J Hyperthermia. 2010;26(3):224–31.
116. Griffin RJ, et al. Mild temperature hyperthermia and radiation therapy: role of tumour vascular thermotolerance and relevant physiological factors. Int J Hyperthermia. 2010;26(3):256–63.
117. Kano E, et al. Effects of hyperthermia at 50 degrees C on V-79 cells in vitro. J Radiat Res. 1982;23(2):218–27.
118. Hainfeld JF, et al. Gold nanoparticle hyperthermia reduces radiotherapy dose. Nanomedicine. 2014;10(8):1609–17.

119. Clement GT, White J, Hynynen K. Investigation of a large-area phased array for focused ultrasound surgery through the skull. Phys Med Biol. 2000;45(4):1071–83.
120. Hynynen K, et al. Pre-clinical testing of a phased array ultrasound system for MRI-guided noninvasive surgery of the brain—a primate study. Eur J Radiol. 2006;59(2):149–56.
121. McDannold N, et al. Evaluation of three-dimensional temperature distributions produced by a low-frequency transcranial focused ultrasound system within ex vivo human skulls. IEEE Trans Ultrason Ferroelectr Freq Control. 2010;57(9):1967–76.
122. Yu VY, et al. Incorporating cancer stem cells in radiation therapy treatment response modeling and the implication in glioblastoma multiforme treatment resistance. Int J Radiat Oncol Biol Phys. 2015;91(4):866–75.
123. Cohen-Inbar O, Xu Z, Sheehan JP. Focused ultrasound-aided immunomodulation in glioblastoma multiforme: a therapeutic concept. J Ther Ultrasound. 2016;4:2.
124. Sapareto SA, Dewey WC. Thermal dose determination in cancer-therapy. Int J Radiat Oncol Biol Phys. 1984;10(6):787–800.
125. Law MP, Ahier RG, Field SB. Response of mouse ear to heat applied alone or combined with X-rays. Br J Radiol. 1978;51(602):132–8.
126. Cetin IA, et al. Retrospective analysis of linac-based radiosurgery for arteriovenous malformations and testing of the Flickinger formula in predicting radiation injury. Strahlenther Onkol. 2012;188(12):1133–8.
127. Burgess A, Hynynen K. Noninvasive and targeted drug delivery to the brain using focused ultrasound. ACS Chem Neurosci. 2013;4(4):519–26.
128. Burgess A, et al. Focused ultrasound-mediated drug delivery through the blood–brain barrier. Expert Rev Neurother. 2015;15(5):477–91.
129. Liu HL, et al. Blood–brain barrier disruption with focused ultrasound enhances delivery of chemotherapeutic drugs for glioblastoma treatment. Radiology. 2010;255(2):415–25.
130. Wei KC, et al. Focused ultrasound-induced blood–brain barrier opening to enhance temozolomide delivery for glioblastoma treatment: a preclinical study. PLoS One. 2013;8(3), e58995.
131. Ting CY, et al. Concurrent blood–brain barrier opening and local drug delivery using drug-carrying microbubbles and focused ultrasound for brain glioma treatment. Biomaterials. 2012;33(2):704–12.
132. Burgess A, Hynynen K. Microbubble-assisted ultrasound for drug delivery in the brain and central nervous system. Adv Exp Med Biol. 2016;880:293–308.
133. Verma J, Lal S, Van Noorden CJ. Nanoparticles for hyperthermic therapy: synthesis strategies and applications in glioblastoma. Int J Nanomedicine. 2014;9:2863–77.
134. Yao MH, et al. Multifunctional Bi2S3/PLGA nanocapsule for combined HIFU/radiation therapy. Biomaterials. 2014;35(28):8197–205.
135. McDaniel JR, et al. Rational design of "heat seeking" drug loaded polypeptide nanoparticles that thermally target solid tumors. Nano Lett. 2014;14(5):2890–5.
136. Fujishiro S, et al. Increased heating efficiency of hyperthermia using an ultrasound contrast agent: a phantom study. Int J Hyperthermia. 1998;14(5):495–502.
137. Top CB, White PJ, McDannold NJ. Nonthermal ablation of deep brain targets: a simulation study on a large animal model. Med Phys. 2016;43(2):870.
138. Arvanitis CD, et al. Cavitation-enhanced nonthermal ablation in deep brain targets: feasibility in a large animal model. J Neurosurg. 2016;124(5):1450–9.
139. Salomir R, et al. Local hyperthermia with MR-guided focused ultrasound: spiral trajectory of the focal point optimized for temperature uniformity in the target region. J Magn Reson Imaging. 2000;12(4):571–83.
140. Liu HL, et al. A novel strategy to increase heating efficiency in a split-focus ultrasound phased array. Med Phys. 2007;34(7):2957–67.
141. Zhou Y. Generation of uniform lesions in high intensity focused ultrasound ablation. Ultrasonics. 2013;53(2):495–505.
142. Partanen A, et al. Reduction of peak acoustic pressure and shaping of heated region by use of multifoci sonications in MR-guided high-intensity focused ultrasound mediated mild hyperthermia. Med Phys. 2013;40(1):013301.
143. Tillander M, et al. High intensity focused ultrasound induced in vivo large volume hyperthermia under 3D MRI temperature control. Med Phys. 2016;43(3):1539–49.
144. Borasi G, et al. Cancer therapy combining high-intensity focused ultrasound and megavoltage radiation. Int J Radiat Oncol Biol Phys. 2014;89(4):926–7.